Heliyon 10 (2024) e25442

Contents lists available at ScienceDirect

Heliyon

journal homepage: www.cell.com/heliyon

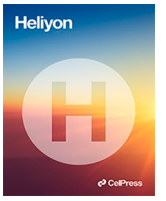

Research article

Enhancing the dielectric and thermal properties of polytetrafluoroethylene-based composites through designing and constructing a novel interfacial structure

Xin Li, Jie Shen, Jing Zhou, Changqing Zhu, Wen Chen *

State Key Laboratory of Advanced Technology for Materials Synthesis and Processing, School of Materials Science and Engineering, Wuhan University of Technology, Wuhan, 430070, PR China

ARTICLE INFO

Keywords:
PTFE-Based composites
Physical interaction
Interfacial structure
Micro-mesoporous SiO_2

ABSTRACT

Polytetrafluoroethylene (PTFE) is widely used as a fundamental core material for high-frequency and high-speed signal transmission fields due to its excellent dielectric properties. However, the high coefficient of thermal expansion (CTE) characteristic of PTFE severely limits its practical application. The CTE of PTFE can be reduced by filling with SiO_2, which is always accompanied by a rapid deterioration of dielectric properties due to the poor interfacial compatibility between SiO_2 and PTFE matrix. In this paper, the challenge of synergistic regulation of dielectric and CTE properties for PTFE-based composites is overcome by constructing an interfacial structure with physical interactions. Micro-mesoporous SiO_2 ($mSiO_2$) is prepared and introduced as a filler, compared with smooth surface SiO_2 ($sSiO_2$), the presence of micro-mesoporous in $mSiO_2$ allows PTFE molecular chains to be adsorbed on the surface or in the pore channels of $mSiO_2$, which improves the interfacial combination of the $mSiO_2$/PTFE composites through the physical interaction between $mSiO_2$ and PTFE. The results show that $mSiO_2$/PTFE composite exhibits a lower CTE (58 ppm $^{\circ}C^{-1}$) while maintaining a lower dielectric constant (ε_r, 2.29, 30 GHz) with dielectric loss (tan δ, 2.31 $\times$ 10^{-3}, 30 GHz) at a filler addition of 30 vol%, as compared with that of the $sSiO_2$/PTFE composites. This work provides a new strategy for fabricating PTFE-based composites with low CTE as well as low ε_r and tan δ.

1. Introduction

The rapid development of the fifth-generation mobile communication technology (5G) and the Internet of Things (IoT) has led to their widespread application in fields such as satellite communication, radar detection, and communication stations [1,2]. As the fundamental core material for the aforementioned electronic devices, the microwave dielectric substrate possesses low dielectric constant (ε_r) and dielectric loss (tan δ), which is a necessary condition for high-quality signal transmission in high-frequency (> 5 GHz) and high-speed (> 10 Gbps) environments [3,4]. Polytetrafluoroethylene (PTFE) substrate is an ideal microwave dielectric substrate that has attracted significant attention due to its low dielectric constant (ε_r, ~2.1) and low dielectric loss (tan δ, ~3.0 $\times$ 10^{-4}) [5–7]. Unfortunately, PTFE has a high coefficient of thermal expansion (CTE, 109 ppm $^{\circ}C^{-1}$) [8,9], which always results in device failure because of excessive CTE.

* Corresponding author.
E-mail address: chenw@whut.edu.cn (W. Chen).

https://doi.org/10.1016/j.heliyon.2024.e25442
Received 27 October 2023; Received in revised form 18 January 2024; Accepted 26 January 2024
Available online 29 January 2024

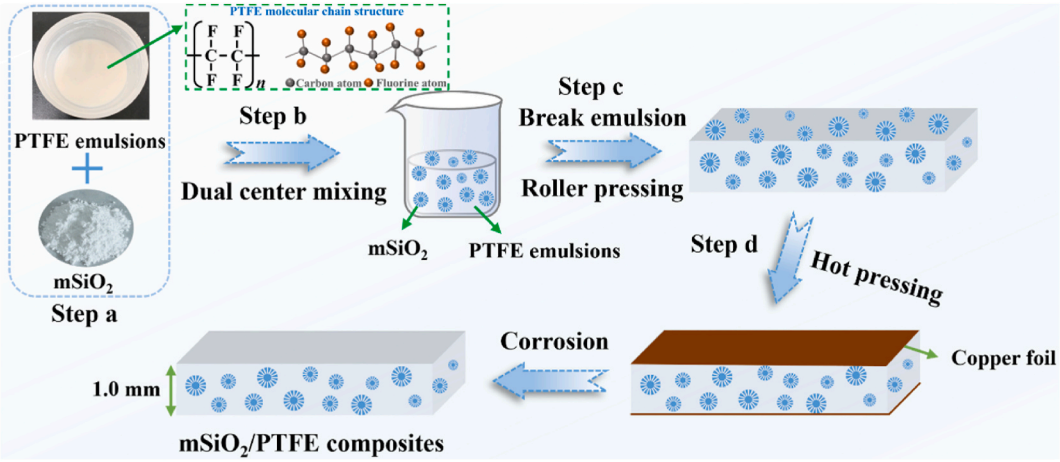

Fig. 1. Schematic diagram of $mSiO_2$/PTFE fabrication.

It is an effective strategy to reduce the CTE of PTFE by filling inorganic fillers [9,10], where SiO_2 becomes an ideal filler due to its relatively low dielectric properties (ε_r, ~4.0, tan δ, ~2.5 × 10^{-3}) and extremely low CTE (~0.5 ppm $°C^{-1}$) [11,12]. However, the reduction of the CTE of SiO_2/PTFE composites is always accompanied by a rapid deterioration of the tan δ, which is attributed to the huge difference between the surface properties of inorganic SiO_2 and organic PTFE, resulting in poor interfacial combination between the filler and the matrix [12,13]. To overcome the above issue of poor interfacial combination, researchers usually modified the filler surface by introducing chemical coupling agents to improve the interfacial compatibility between the filler and the matrix [11,14,15]. Regrettably, the chemical modification process inevitably introduces polar bonds, which causes the tan δ of composites to increase rapidly in high-frequency conditions [16]. Consequently, it is essential to develop an interfacial structure modification strategy that does not introduce coupling agents to meet the application requirements of composites in high-frequency and high-speed fields.

Some researchers have found in other polymer systems by constructing and using a porous filler to composite with the polymer matrix, the porous structure of the filler can be utilized to form effective physical interactions with the polymer matrix, thereby improving the interfacial combination of the filler and the matrix. For example, Sun et al. investigated the variation of interfacial combination of porous limestone filler with asphalt matrix, and the results showed that filler porosity is an essential factor affecting asphalt-filler interfacial interaction [17]. Run et al. used in situ polymerization to prepare poly (methyl methacrylate)/mesoporous molecular sieve (PMMA/MMS) composites. The results demonstrated that the interfacial interaction force between the filler and the polymer resin is improved due to the physical interpenetration effect between the organic polymer chains and the mesoporous molecular sieves [18]. Yu et al. found that the molecular chains of the epoxy resin can be introduced into the channels of the mesoporous SiO_2 to form a tightly combined structure [19]. It can be seen that the introduction of fillers containing porous structure can physically adsorb polymer molecular chains, enabling the polymer molecular chains to be adsorbed on the surface of the porous structure or into the pore channels, forming a physical interaction interface structure, thus improving the interfacial combination of fillers and the matrix without coupling agents.

Inspired by the above viewpoints, here, SiO_2 with micro-mesoporous ($mSiO_2$) was prepared and introduced into PTFE to fabricate novel $mSiO_2$/PTFE composites. $mSiO_2$ possesses micro-mesoporous that can physically adsorb PTFE molecular chains, which results in a stronger interfacial interaction force between $mSiO_2$ and PTFE, as compared with smooth surface SiO_2 ($sSiO_2$). In this paper, the microstructure, interfacial combination, dielectric, and thermal properties of $mSiO_2$/PTFE composites were systematically investigated.

2. Experimental section

2.1. Reagents

The raw materials were polytetrafluoroethylene (PTFE) aqueous dispersion (60 wt%, TE-3865C, Dupont, USA). Tetraethyl orthosilicate (TEOS), aqueous ammonia solution ($NH_3·H_2O$, 28 wt%), cetyltrimethylammonium bromide (CTAB), and ethanol (C_2H_5OH) were all analytically pure (A.R.), supplied by Sinopharm Chemical Reagent Co., Ltd., P.R. China. Deionized water was prepared in our laboratory and applied in all reaction and treatment processes.

2.2. Preparation of $sSiO_2$ and $mSiO_2$ powders

$sSiO_2$ with an approximate particle diameter of 0.97 μm was prepared based on Ref. [20]. The preparation process of $mSiO_2$ was as follows: Firstly, the water bath temperature was fixed at 10 °C, the molar ratio of TEOS:$NH_3·H_2O$:H_2O:C_2H_5OH:CTAB was 1:19:370:230:0.2, and the reaction time was 2.5 h. After the reaction was finished, it was washed with deionized water for many times,

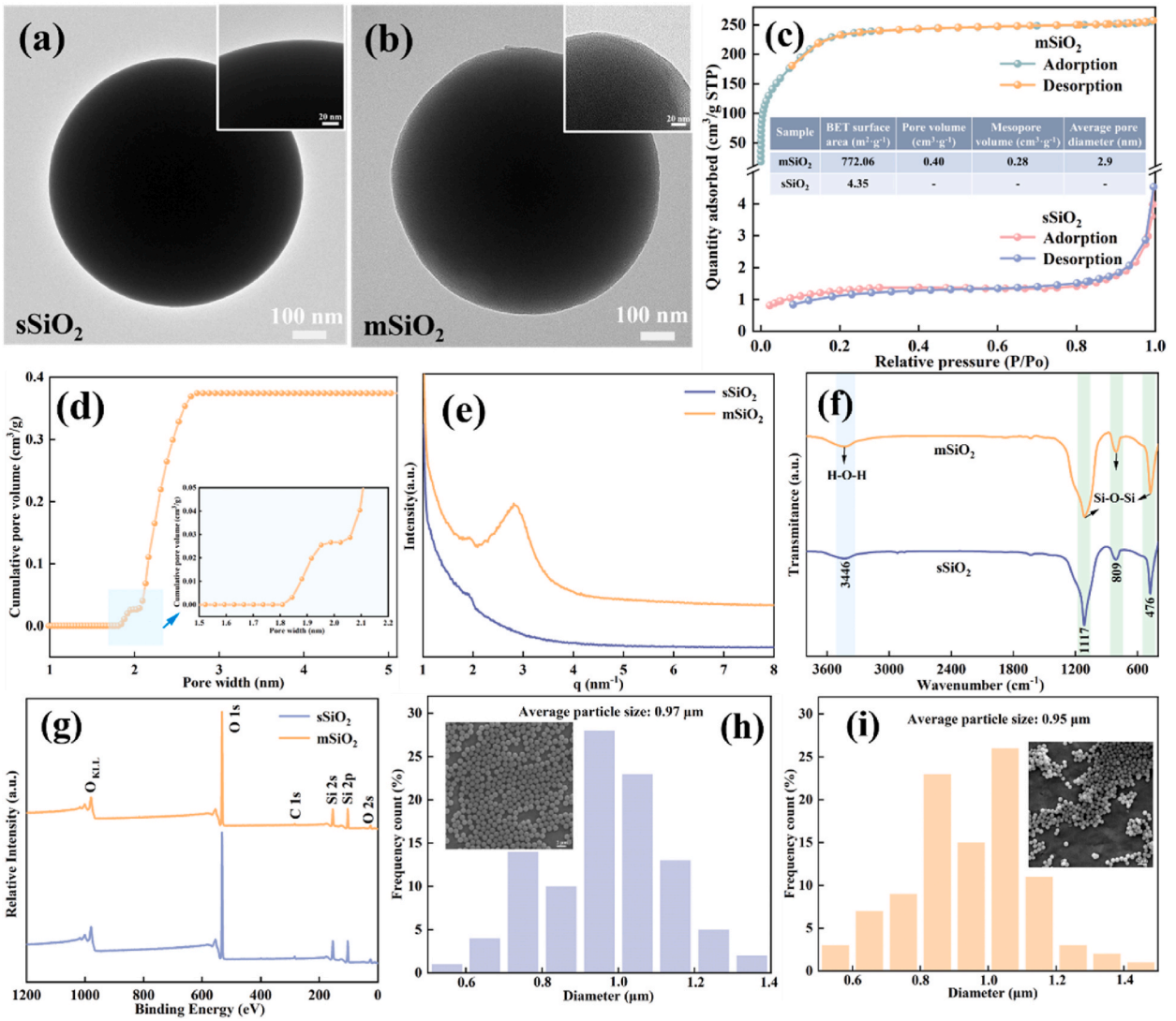

Fig. 2. TEM images, (a) $sSiO_2$, (b) $mSiO_2$. Adsorption-desorption isotherms of $sSiO_2$ and $mSiO_2$ (c). Pore size-accumulated pore volume plots of $mSiO_2$ (d). Small-angle X-ray scattering patterns of $sSiO_2$ and $mSiO_2$ (e). FTIR spectra of $sSiO_2$ and $mSiO_2$ (f). XPS spectra of $sSiO_2$ and $mSiO_2$ (g). Statistical diagrams of particle size based on inset SEMs, (h) $sSiO_2$, (i) $mSiO_2$.

then dried at 80 °C for 10 h, and finally, the powder was calcined in a muffle furnace at 750 °C for 5 h to obtain $mSiO_2$. $mSiO_2$ synthesis process is shown in Fig. S1.

2.3. Preparation of SiO_2/PTFE composites

SiO_2/PTFE composites were synthesized in the following steps: Step a, the $sSiO_2$ and $mSiO_2$ powders were added to PTFE aqueous dispersions with a solid content of 60 wt%, respectively. Step b, the SiO_2 powder and PTFE were thoroughly stirred on a double-center mixer for 3 min. Step c, ethanol was added to break the emulsion to obtain organic-inorganic blends containing certain volumes of SiO_2 (20 vol%, 30 vol%, and 40 vol%), the above organic-inorganic blend was calendered to obtain a composite pre-pressed sheet with a thickness of 1 mm, and the pre-pressed sheet was dried at 180 °C for 48 h. Step d, the dried pre-pressed sheet, and the copper foil were hot pressed at 385 °C for 2 h to obtain a copper-clad laminate, which was then corroded with $FeCl_3{\cdot}6H_2O$ solution to obtain the SiO_2/PTFE composites. $sSiO_2$/PTFE was prepared in the same process as the $mSiO_2$/PTFE, as shown in Fig. 1.

2.4. Characterizations

The microstructures of fillers were investigated using a transmission electron microscope (TEM, JEM-1400Plus, JEOL, Japan). The interfacial combination of composites was observed using a transmission electron microscope (TEM, JEM-1400Plus, JEOL, Japan) and

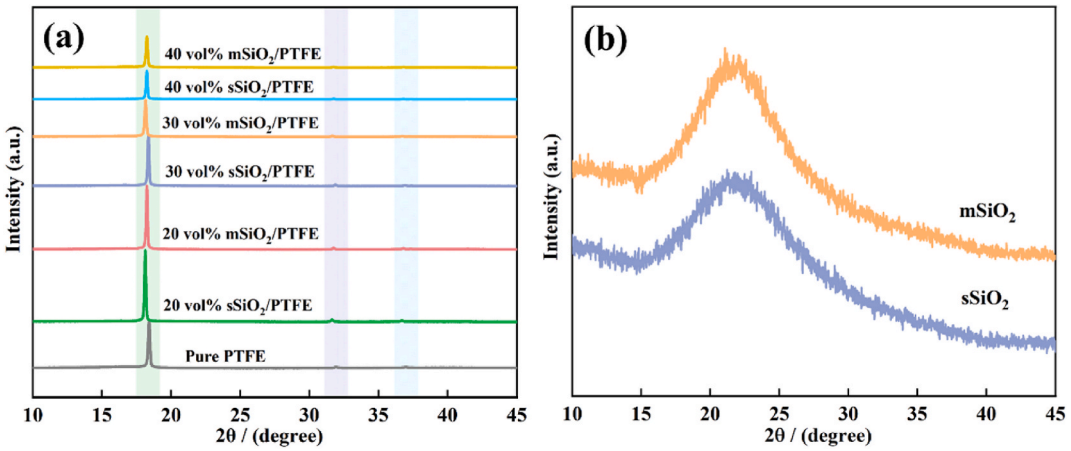

Fig. 3. XRD patterns, (a) composites, (b) $sSiO_2$ and $mSiO_2$.

a field emission scanning electron microscope (FESEM, JSM-7500F, JEOL, Japan). Among them, the interfacial combination observed by TEM is the composites processed by ultrathin slicing to a thin slice of about 100 nm. The particle size and distribution of $sSiO_2$ and $mSiO_2$ in the FESEM images were analyzed using IMAGE J software. The chemical structures of $sSiO_2$ and $mSiO_2$ powders were characterized using a Fourier transform infrared spectrometer (FTIR, Lambda 750S, PerkinElmer, America) in the range of 400–4000 cm^{-1}. X-ray diffraction (XRD) data of the samples were collected using a Cu Kα (45 kV, 35 mA) radiation diffractometer (Miniflex 600, Rigaku, Japan). The scanning range was from 5° to 50°, and the scanning speed was $5°{\cdot}min^{-1}$. The chemical elements on the surface of $sSiO_2$ and $mSiO_2$ fillers were analyzed using X-ray photoelectron analysis (XPS, ESCALAB 250Xi, Thermo Scientific, America). The pore structure characteristics of $sSiO_2$ and $mSiO_2$ were characterized using a small-angle X-ray scattering (SAXS, EMPYREAN, Panalytical, Netherlands).

Dynamic mechanical analysis (DMA, DMA8000, PerkinElmer, America) was performed in three-point bending mode. The experiments were carried out using a liquid nitrogen cooling device, and the measurements were performed in the temperature range of −50 °C–200 °C with a heating rate of 5 $°C{\cdot}min^{-1}$. The melting temperature (T_m) and melting enthalpy (ΔH_m) of $sSiO_2$/PTFE and $mSiO_2$/PTFE composites were determined by differential scanning calorimetry (DSC, DSC8500, PerkinElmer, America). The test range was from room temperature to 380 °C with a rate of 5 $°C{\cdot}min^{-1}$ in air. Tensile stress was determined using an Instron-type mechanical testing machine (Instron 5967, Instron, America). The tensile rate was 10 mm min^{-1}, and the test temperature was 25 °C. All data were averaged over at least three samples.

The coefficients of thermal expansion (CTE) data of $sSiO_2$/PTFE and $mSiO_2$/PTFE composites were collected by testing the *Z*-axis using a thermomechanical analyzer (TMA202, Netzsch, Germany) under an N_2 atmosphere in the range of 0 °C–100 °C with a heating rate of 5 $°C{\cdot}min^{-1}$. The dielectric data of $sSiO_2$/PTFE and $mSiO_2$/PTFE composites were collected using a vector network analyzer (8722 ET, Agilent, America) in the range of 5–30 GHz. The dielectric and CTE properties measurements were performed according to the IPC-TM-650 test method manual. The characterizations of PTFE-based composites with a filler addition of 30 vol% are represented when not stated specifically.

3. Results and discussion

3.1. *$sSiO_2$ and $mSiO_2$ powders*

Fig. 2(a) and (b) show the TEM images of $sSiO_2$ and $mSiO_2$. It can be observed that $sSiO_2$ does not exhibit any pore channels, whereas $mSiO_2$ clearly shows the presence of micro-mesoporous channels. Furthermore, Fig. 2(c) presents the adsorption-desorption isotherms of $sSiO_2$ and $mSiO_2$ obtained from BET testing. It can be seen that $mSiO_2$ exhibits a type I adsorption-desorption isotherm, corresponding to a micro-mesoporous structure. $sSiO_2$ refers to a type III adsorption-desorption isotherm, indicating that $sSiO_2$ is basically non-adsorbed and is a non-porous channel material. As indicated in the inset table of Fig. 2(c), it reveals that $mSiO_2$ possesses a porous structure with an average pore size of 2.9 nm, and a significantly higher specific surface area than $sSiO_2$. This is consistent with the cumulative pore volume in Fig. 2(d), which shows a gradual increase starting from slightly below a pore diameter of 2 nm, followed by a rapid increase after 2 nm. The SAXS patterns (Fig. 2(e)) also show that $mSiO_2$ possesses a micro-mesoporous structure, while $sSiO_2$ has no pore channel structure [21,22]. The FTIR spectra in Fig. 2(f) reveal that $sSiO_2$ has the same surface chemical structure as $mSiO_2$, with only Si–*O*–Si and H–*O*–H bonds, and no additional polar bonds are introduced. The XPS spectra (Fig. 2(g)) also demonstrate that $sSiO_2$ and $mSiO_2$ contain the same chemical elements. In addition, $sSiO_2$ and $mSiO_2$ have similar particle size distributions and average particle sizes (Fig. 2(h) and (i)).

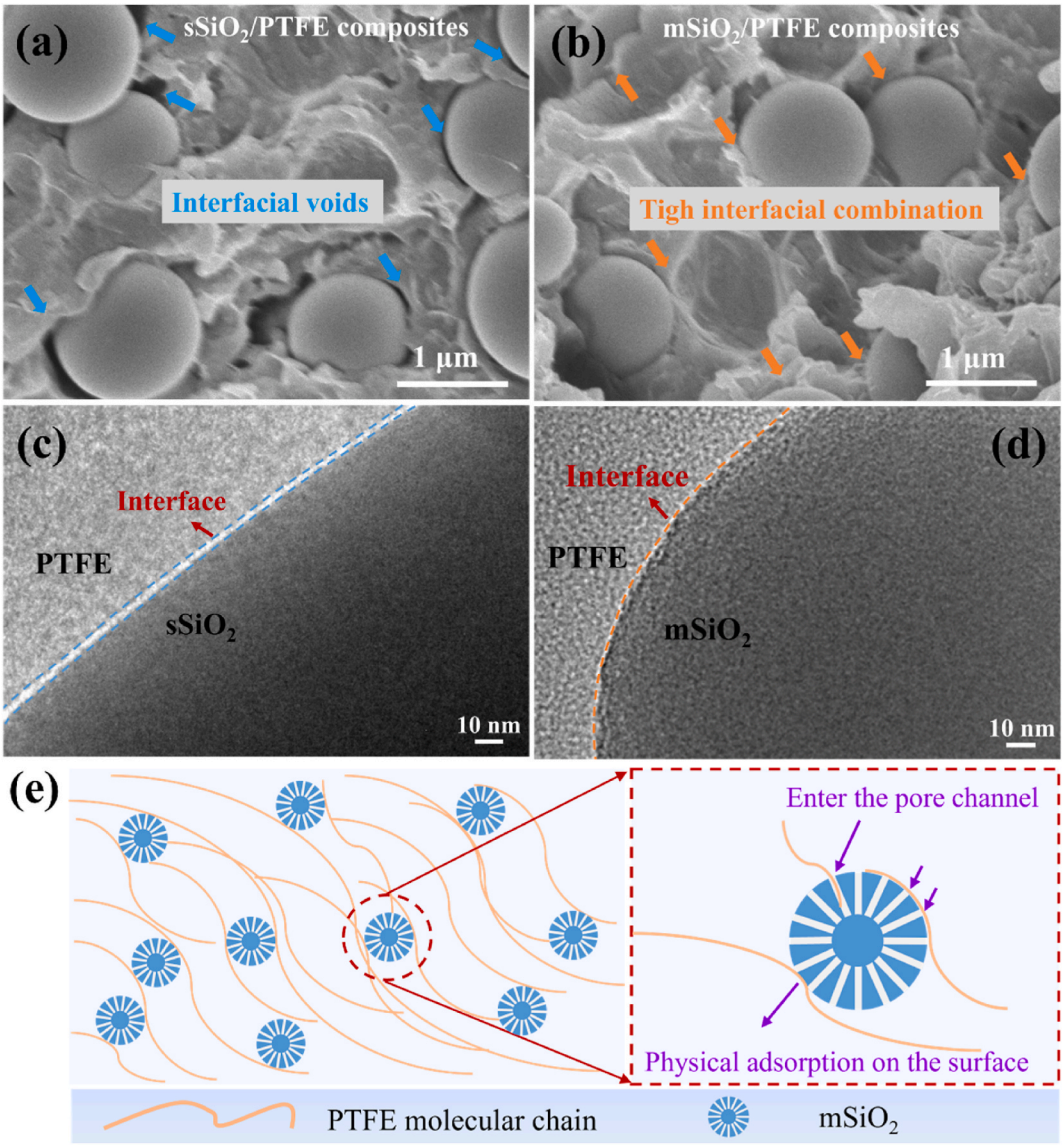

Fig. 4. Cross-sectional FESEM images, (a) $sSiO_2$/PTFE, (b) $mSiO_2$/PTFE. TEM images of ultrathin slices for composites, (c) $sSiO_2$/PTFE, (d) $mSiO_2$/PTFE. Schematic illustration of the physical interaction mechanism between $mSiO_2$ and PTFE molecular chains (e). The PTFE-based composites correspond to $sSiO_2$ and $mSiO_2$ filler additions of 30 vol%, respectively.

3.2. Composites phase structure and interfacial combination

3.2.1. Phase structure

Before analyzing the interfacial combination of the composites, we determined the phase structures of $sSiO_2$/PTFE and $mSiO_2$/PTFE, and the results are shown in Fig. 3(a). As can be seen from the XRD patterns (Fig. 3(a)), $sSiO_2$/PTFE and $mSiO_2$/PTFE have consistent phase structures, which are both shown as the crystalline phases of PTFE [23]. With the increase of fillers, the movement of more PTFE molecular chains is hindered, resulting in a decrease of crystallinity. The SiO_2 phases have not been detected because the $sSiO_2$ and $mSiO_2$ are amorphous phases, which is evident from the broad peaks in Fig. 3(b). The characteristic diffraction peaks of the composites are weakened, which is consistent with the variation trend of the crystallinity of the composites calculated in the subsequent DSC section.

3.2.2. Analyses of interfacial combination from the microstructure of composites

Fig. 4(a) and (b) show the cross-sectional FESEM images of $sSiO_2$/PTFE and $mSiO_2$/PTFE composites. There are obvious voids between the two phases of $sSiO_2$/PTFE, while the $mSiO_2$/PTFE are tightly combined. In addition, we made ultra-thin slicing of $sSiO_2$/PTFE and $mSiO_2$/PTFE to observe the interfacial combination of filler ($sSiO_2$ and $mSiO_2$) and matrix (PTFE), respectively. Among

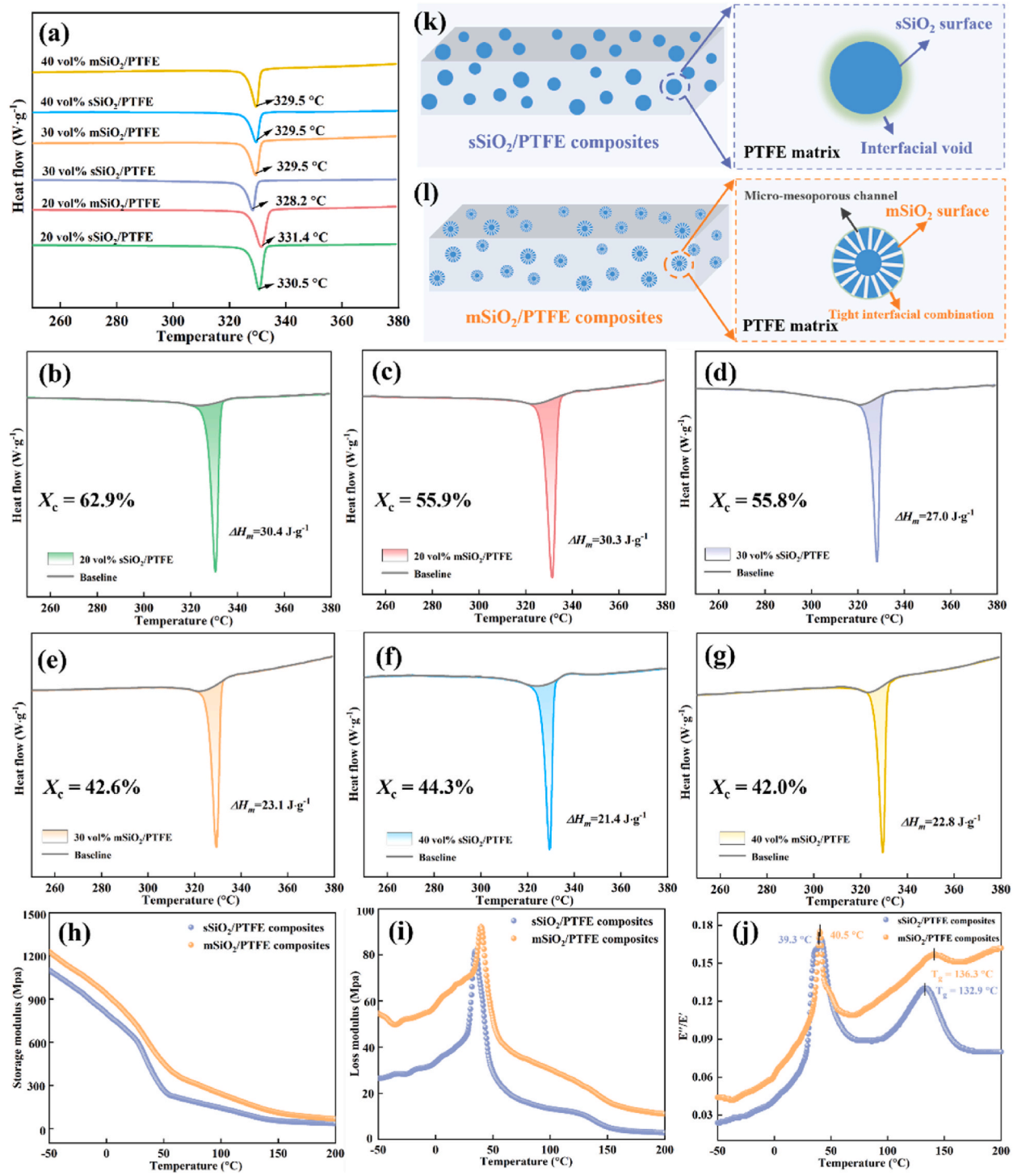

Fig. 5. DSC curves of composites (a). The melt enthalpies of composites are obtained based on DSC tests, (b,d,f) $sSiO_2$/PTFE, (c,e,g) $mSiO_2$/PTFE. DMA curves of composites, E′ (h), E″ (i), E″/E′ (j). Schematic illustration of interfacial combination for composites, $sSiO_2$/PTFE (k), $mSiO_2$/PTFE (l). DMA tests of PTFE-based composites are carried out at 30 vol% addition of $sSiO_2$ and $mSiO_2$ fillers, respectively.

them, Fig. 4(c) shows the high-magnification TEM image of $sSiO_2$/PTFE, and Fig. 4(d) refers to the high-magnification TEM images of $mSiO_2$/PTFE. The low-magnification TEM images of the composites are shown in Fig. S2. The existence of interfacial voids between $sSiO_2$ and PTFE can be clearly seen in Fig. 4(c), while no apparent interfacial voids between $mSiO_2$ and PTFE are observed in Fig. 4(d). This result indicates that $mSiO_2$/PTFE has a tighter interfacial combination, which is consistent with the results of FESEM analysis.

Table 1
T_m, ΔH_m, and X_c of PTFE-based composites.

Filler	Loading	T_m (°C)	ΔH_m (J·g^{-1})	X_c (%)
$sSiO_2$	20 vol%	330.5	30.4	62.9
	30 vol%	328.2	27.0	55.8
	40 vol%	329.5	21.4	44.3
$mSiO_2$	20 vol%	331.4	30.3	55.9
	30 vol%	329.5	23.1	42.6
	40 vol%	329.5	22.8	42.0

$mSiO_2$/PTFE exhibits a better interfacial combination than $sSiO_2$/PTFE for the following reasons: The molecular chains of the molten state PTFE are in motion during the hot-pressing process of composites, and the PTFE molecular chains (the diameter is around 0.27 nm [24]) encounter the micro-mesoporous channels of the $mSiO_2$ filler (average pore size is 2.9 nm), the physical adsorption generated by the micro-mesopores may cause a portion of the PTFE molecular chains to adsorb onto the surface of $mSiO_2$, while another portion of the molecular chains enters the micro-mesoporous channels of $mSiO_2$ (the interaction schematic as illustrated in Fig. 4(e)). At this time, the movement of the PTFE molecular chains is impeded. After the hot pressing is completed, the PTFE molecular chains form a tight physical interaction with $mSiO_2$ due to the force generated by physical adsorption, constructing an interface structure with an excellent interfacial combination at the interface of $mSiO_2$/PTFE composites. In contrast, the interfacial combination of $sSiO_2$/PTFE composites is poor due to the absence of micro-mesoporous channels in $sSiO_2$, which cannot produce effective physical adsorption with the PTFE molecular chains.

3.2.3. Analyses of interfacial combination for composites from the thermodynamic perspective

To further analyze the interfacial combination of composites as well as to reveal the interfacial interaction mechanism of composites, we performed DSC and DMA tests on $sSiO_2$/PTFE and $mSiO_2$/PTFE. Fig. 5(a) shows the DSC curves of $sSiO_2$/PTFE and $mSiO_2$/PTFE composites, from which it can be seen that there is no significant difference in the melting temperatures (T_m) of $sSiO_2$/PTFE and $mSiO_2$/PTFE composites, which floats within the range of 328.2–331.4 °C. It is more noteworthy that the melting enthalpies (ΔH_m) of the composites based on the DSC tests are shown in Fig. 5(b)–5(g). Based on Eq. (1), the crystallinity (X_c) of $sSiO_2$/PTFE is calculated to be 62.9 %, 55.8 %, and 44.3 % for filler contents of 20 vol%, 30 vol%, and 40 vol%, respectively, whereas the X_c of $mSiO_2$/PTFE is significantly lower, with 55.9 %, 42.6 %, and 42.0 % (the specific data are listed in Table 1), the X_c of $sSiO_2$/PTFE and $mSiO_2$/PTFE gradually decrease with the increase of filler, which is also due to the impediment of the movement of more PTFE molecular chains, and this is consistent with the variation trend of the composites' characteristic diffraction peaks in the above XRD analyses. In addition, the X_c of $mSiO_2$/PTFE is lower than that of $sSiO_2$/PTFE at the same content of filler, which suggests that the interfacial combination of $mSiO_2$ and PTFE is more closely combined due to the presence of pore channels in the $mSiO_2$, thus enabling the $mSiO_2$ to better hinder the movement of PTFE molecular chain.

$$X_c = \frac{\Delta H_m}{\varphi_m \Delta H_m^o} \tag{1}$$

Where φ_m is the mass fraction content of PTFE, ΔH_m^o is the melting enthalpy of pure PTFE, 69.0 J g^{-1} [25,26], ΔH_m refers to the melting enthalpy of the composites obtained from the DSC. The ΔH_m of $sSiO_2$/PTFE and $mSiO_2$/PTFE are listed in Table 1, respectively. Based on the given densities of PTFE, $sSiO_2$, and $mSiO_2$ as 2.20 g cm^{-3}, 2.20 g cm^{-3} [27], and 1.39 g cm^{-3} (Fig. S3), respectively, and with a filler addition of 30 vol%, the corresponding filler mass fraction contents for $sSiO_2$/PTFE and $mSiO_2$/PTFE composites are 30.0 wt% and 21.4 wt%, respectively.

Fig. 5(h)–5(j) correspond to the diagrams of energy storage modulus (E′), loss modulus (E″), and loss factor (E″/E′) obtained from the DMA tests of $sSiO_2$/PTFE and $mSiO_2$/PTFE composites. A higher E′ indicates a stronger rigidity of the system [28,29], while a higher E″ represents a stronger obstruction to the motion of the polymer molecular chains in the system, resulting in a larger energy loss in the motion of the polymer molecular chains [30,31]. As can be seen from Fig. 5(h) and (i), the E′ and E″ of $sSiO_2$/PTFE are 36.6–1098.5 MPa and 2.9–81.6 MPa at -50–200 °C, respectively, while those of $mSiO_2$/PTFE with 68.4–1227.3 MPa and 11.0–92.2 MPa, $mSiO_2$/PTFE have higher E′ and larger E″ than $sSiO_2$/PTFE, indicating that the $mSiO_2$/PTFE more tightly combined with better interfacial combination, the rigidity of the $mSiO_2$/PTFE system is increased, and the movement of PTFE molecular chains produces more energy loss. Fig. 5(j) shows the E″/E′ patterns, the first peak is the change of the PTFE molecular chain from helical conformation to irregular winding in SiO_2/PTFE composites [32], the peak position of $sSiO_2$/PTFE is 39.3 °C whereas that of $mSiO_2$/PTFE is 40.5 °C. The increase of 1.2 °C may be related to the tighter interfacial combination of $mSiO_2$/PTFE than $sSiO_2$/PTFE. The second peak refers to the glass transition temperature (T_g) peak of the composites [33]. It can be clearly seen that the T_g of $mSiO_2$/PTFE is 136.3 °C, higher than that of 132.9 °C for $sSiO_2$/PTFE, and it can also indicate that the $mSiO_2$ has stronger interfacial interactions with PTFE, which makes the $mSiO_2$/PTFE have a closer interfacial combination. Schematic illustrations of the composites interface combination as shown in Fig. 5(g) and (h).

3.2.4. Analyses of interfacial combination for composites from the mechanical perspective

Mechanical characterization and simulation are also effective ways to analyze and reveal composites' interfacial combination and interfacial interaction mechanism. Fig. 6(a) and (b) show the tensile stress-strain curves of $sSiO_2$/PTFE and $mSiO_2$/PTFE at different

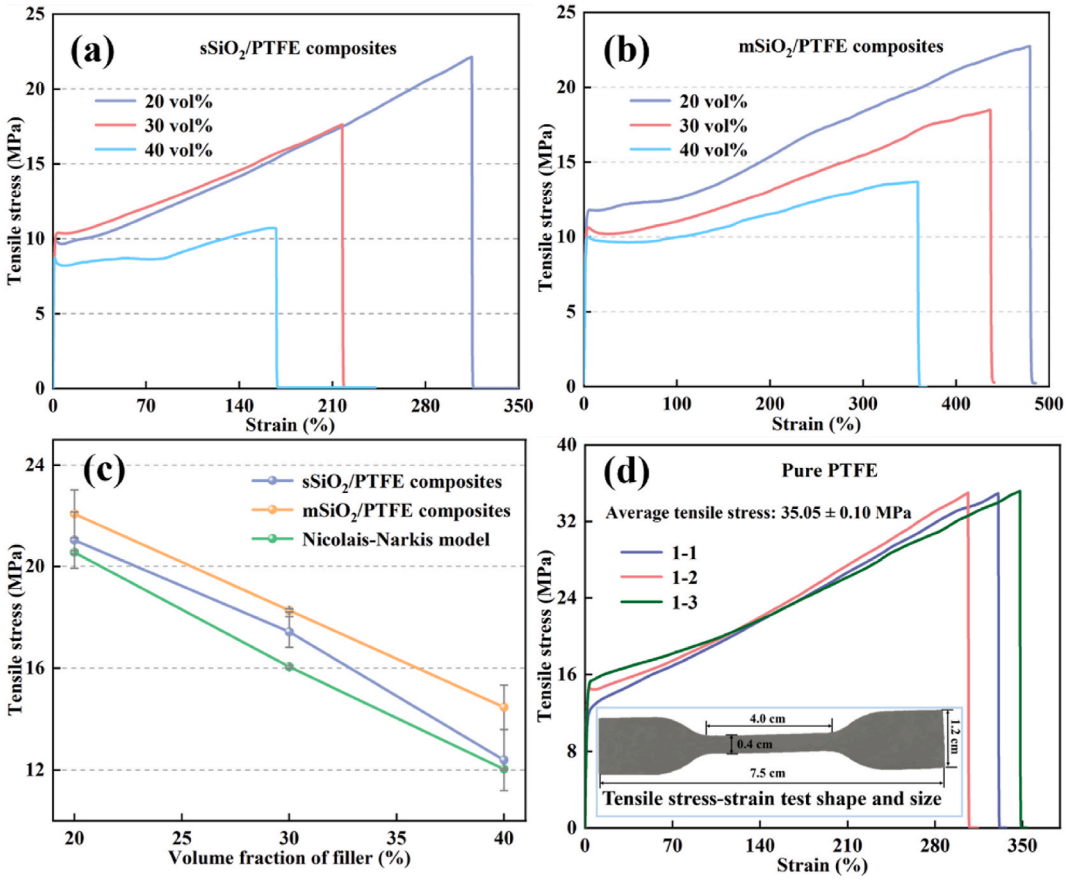

Fig. 6. Tensile stress-strain curves of composites, $sSiO_2$/PTFE (a), $mSiO_2$/PTFE (b). Composites tensile stress test and theoretical values (c). The tensile stress-strain curves of pure PTFE (d).

volumes of SiO_2 filler addition (20 vol%, 30 vol%, and 40 vol%). The tensile stress (σ_c) of $mSiO_2$/PTFE is stronger than $sSiO_2$/PTFE at the same filler addition content (Fig. 6(c)), which demonstrates that $mSiO_2$/PTFE has stronger interfacial interactions. To further detect the differences in interfacial interactions in the SiO_2/PTFE composites mentioned above, the theoretical model for the dependence of σ_c on filler volume fraction proposed by Nicolais and Narkis is used, which can be expressed as Eq. (2) [33,34].

$$\sigma_c = \sigma_m\left(1 - 1.21\Phi_f^{\frac{2}{3}}\right) \tag{2}$$

where σ_c and σ_m represent the tensile stress of the composites and pure PTFE, respectively, and Φ_f refers to the volume fraction of filler. The tensile stress-strain curves of pure PTFE are presented in Fig. 6(d).

The data calculated by Eq. (2) are presented in Fig. 6(c), in which the spherical rigid particles are assumed to be uniformly dispersed between the filler and the polymer matrix without any interfacial interaction force between the two phases [35]. σ_c experimental values of $sSiO_2$/PTFE and $mSiO_2$/PTFE composites are higher than the theoretical values, among them, σ_c of $sSiO_2$/PTFE is higher than the theoretical value, which demonstrates that $sSiO_2$ utilizes its own volume effect to produce certain interaction with PTFE. What is more noteworthy that the σ_c of $mSiO_2$/PTFE is not only higher than the theoretical value, but also greater than that of $sSiO_2$/PTFE, which is a sufficient indication that the $mSiO_2$ produces stronger interfacial interactions with PTFE due to the presence of pore-channel structure.

In terms of the theoretical mechanical model, a tighter interfacial combination of the composites provides a greater stiffness of the composite system, which is reflected in a more uniform stress (tensile force per unit area) distribution at the interface between the two phases in the composites when an external tensile stress is applied to the composites [36]. Based on the solid mechanics model in COMSOL 6.1 software, a two-dimensional SiO_2/PTFE composites model with a length × width of 5 μm × 5 μm is constructed, in which the area of the PTFE matrix model occupied by $sSiO_2$ and $mSiO_2$ fillers is 30 %, respectively, and the stress distributions of the $sSiO_2$/PTFE and $mSiO_2$/PTFE composites at the interface as well as between the filler particles are calculated by fixing the bottom side of the model, and then applying different tensile stresses (5,10, and 20 MPa), to the top side of the model, the results are shown in Fig. S4. Fig. S4 exhibits that the uniformity of stress distribution between the filler particles of $mSiO_2$/PTFE is better than that of $sSiO_2$/PTFE at different stresses. As indicated by the red arrows in the area, the color moves in the direction that represents less stress.

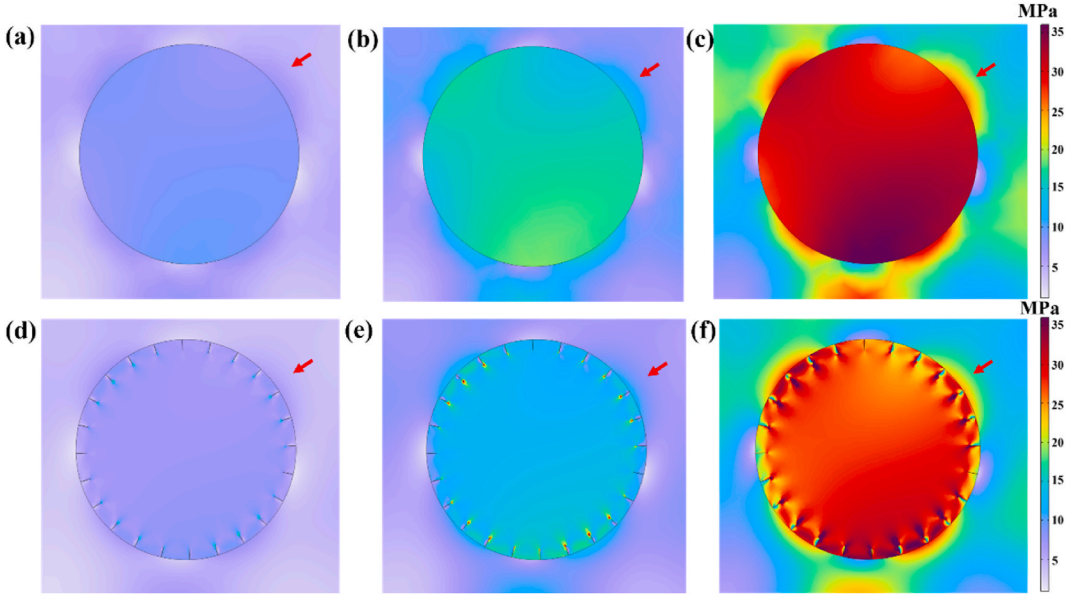

Fig. 7. Stress distribution of composites with a different tensile stress, (a)–(c) corresponding to $sSiO_2$/PTFE, (a) 5 MPa, (b) 10 MPa, (c) 20 MPa. (d)–(f) referring to $mSiO_2$/PTFE, (d) 5 MPa, (e) 10 MPa, (f) 20 MPa.

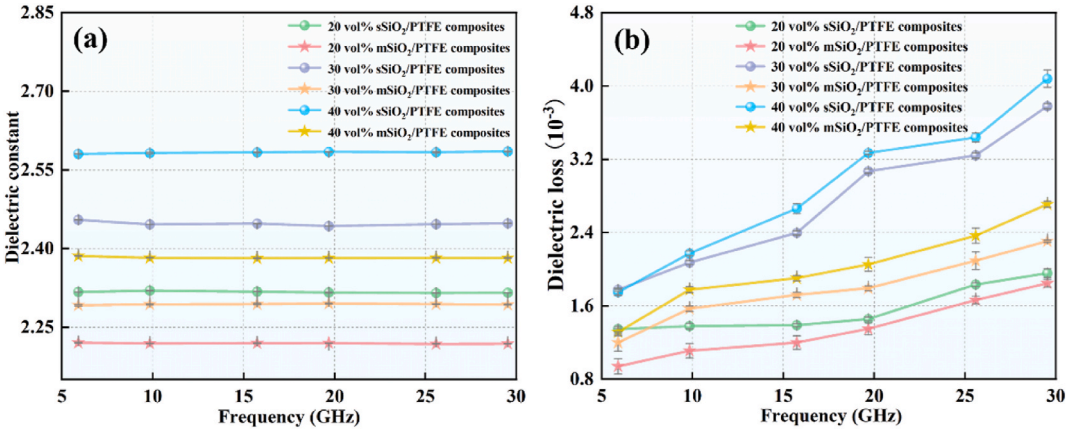

Fig. 8. Dielectric constant of composites (a), dielectric loss for composites (b).

The stress distributions at the interface of a single SiO_2 sphere with the PTFE matrix are exhibited in Fig. 7(a)–7(f), and the red circle in Fig. S4 marks the location of the sphere.

Fig. 7(a)–7(c) reveal that there is a more apparent stress concentration at the $sSiO_2$/PTFE interface (colors are shifted in the direction representing higher stress values), while the stress distribution at the $mSiO_2$/PTFE interface is more uniform (Fig. 7(d)–7(f)), under different stresses. This result is consistent with the above analysis, indicating that the physical interaction force between $mSiO_2$ and PTFE effectively improves the interfacial combination of $mSiO_2$/PTFE, owing to the effective physical adsorption of PTFE molecular chains by the micro-mesoporous of $mSiO_2$. One portion of the PTFE molecular chains is adsorbed on the surface of $mSiO_2$, while another portion of PTFE molecular chains is embedded in the pore channels of $mSiO_2$.

3.3. Dielectric and thermal properties of $sSiO_2$/PTFE and $mSiO_2$/PTFE composites

Maintaining a low ε_r and low tan δ of PTFE-based composites is a performance requirement for their application in high-frequency and high-speed fields. Fig. 8(a) shows that the variation of ε_r is minimal with the change of test frequency (5–30 GHz) for $sSiO_2$/PTFE and $mSiO_2$/PTFE, when the filler content remains constant. This result indicates that PTFE-based composites have stable ε_r at different frequencies. In addition, Fig. 8(a) also shows that as the addition of $sSiO_2$ increases from 20 vol% to 40 vol%, the ε_r of $sSiO_2$/PTFE increases from 2.32 to 2.59 (30 GHz). The increase in ε_r is because the ε_r of SiO_2 is 4.0, which is higher than that of PTFE ($\varepsilon_r = 2.1$),

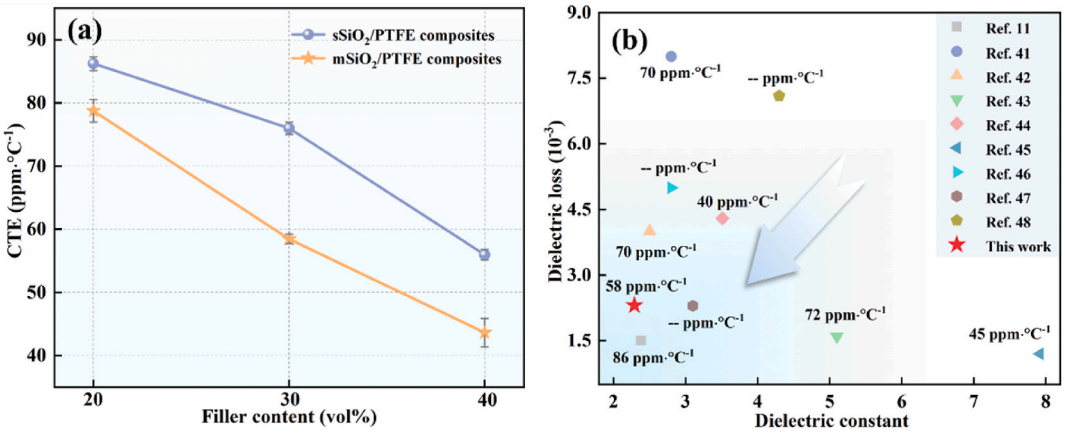

Fig. 9. CTE of composites (a), comparison of dielectric and thermal properties of $mSiO_2$/PTFE composites and published PTFE-based composites (b).

Table 2
Comparison of dielectric and thermal properties with PTFE-based composites.

Filler	Loading	ε_r	tan δ (10^{-3})	f (GHz)	CTE (ppm·°C^{-1})	Ref.
SiO_2	30 vol%	2.38	1.53	40	86	[11]
Mg_2SiO_4	30 vol%	2.8	8.0	5	70	[41]
SiO_2	30 wt%	2.5	4.0	5	70	[42]
BCZN	30 vol%	5.1	1.6	7	72	[43]
$Sm_2Si_2O_7$	30 vol%	3.5	4.3	9	40	[44]
$(Ca,Li,Sm)TiO_3$	40 vol%	7.9	1.2	10	45	[45]
$ZnAl_2O_4$	30 vol%	2.8	5.0	7	–	[46]
$Li_2Mg_3TiO_6$	30 wt%	3.1	2.3	10	–	[47]
Rutile	30 wt%	4.3	7.1	11.5	–	[48]
$mSiO_2$	30 vol%	2.29	2.31	30	58	This work

therefore, the ε_r of the composites increases gradually with the increase in SiO_2 addition. For $mSiO_2$ at the same volume fraction, the ε_r ranges from 2.22 to 2.38 (30 GHz), which is lower than that of $sSiO_2$/PTFE. $mSiO_2$/PTFE possesses a lower ε_r than that of $sSiO_2$/PTFE for the following reasons: On the one hand, the density of $mSiO_2$ is smaller than that of $sSiO_2$ (analytical part of Fig. S3), and at the same volumetric content of filler (e.g., 30 vol%), the density of $mSiO_2$/PTFE composites is smaller than that of $sSiO_2$/PTFE (Table S1), which suggests that when $mSiO_2$ is added as a filler to the PTFE matrix, $mSiO_2$ introduces air ($\varepsilon_r = 1.0$) due to the presence of micro-mesoporous channels. $mSiO_2$/PTFE composites with a tight interfacial combination enable the pore channels to be enclosed, and the air introduced by $mSiO_2$ with an extremely low ε_r is retained. On the other hand, it is because $mSiO_2$/PTFE has a better interfacial combination than $sSiO_2$/PTFE, which results in a smaller relaxation polarization at the $mSiO_2$/PTFE interface [37].

As shown in Fig. 8(b), it can be observed that when the addition amount of $sSiO_2$ is 20–40 vol%, the tan δ of $sSiO_2$/PTFE increases rapidly from 1.96×10^{-3} to 4.08×10^{-3} at 30 GHz. However, for the same filler content, the tan δ of $mSiO_2$/PTFE is significantly lower than that of $sSiO_2$/PTFE, ranging from 1.85×10^{-3} to 2.71×10^{-3} at 30 GHz. The reason for the decrease in tan δ is as follows: The presence of more polar bonds (Si–*O*–Si and H–*O*–H) at the SiO_2 solid-gas interface provides additional polarization loss by the formation of locally aligned dipoles when SiO_2 interfaces poorly with PTFE, whereas $mSiO_2$/PTFE has a tight interfacial combination, which decreases the polarization loss [38].

PTFE-based composites, which are used as core component materials, can cause electronic devices to fail if the CTE is too high [38,39,40]. Therefore, PTFE-based composites with low CTE while maintaining low ε_r and low tan δ are essential to ensure the application of composites. As shown in Fig. 9(a), the CTE curves of the samples with the designed series of filler loading demonstrate a similar decreasing trend in both $sSiO_2$/PTFE and $mSiO_2$/PTFE composites. Nevertheless, an apparent discrepancy exists in the CTE performances between $sSiO_2$/PTFE and $mSiO_2$/PTFE composites. At the same filler addition (20–40 vol%), $mSiO_2$/PTFE has a lower CTE (44–79 ppm °C^{-1}) than $sSiO_2$/PTFE (56–86 ppm °C^{-1}). This phenomenon is attributed to the physical adsorption of PTFE molecular chains by the micro-mesoporous structure of $mSiO_2$, which makes the two-phase interface tightly combined, and when the external test temperature changes, the movement of PTFE molecular chains to generate thermal expansion is more effectively hindered. The results demonstrate that introducing $mSiO_2$ is an effective way to improve the dielectric and CTE properties of PTFE-based composites.

Based on the dielectric and thermal properties of $mSiO_2$/PTFE at $mSiO_2$ addition of 30 vol%, we compare the results with the reported PTFE-based composites (with close filler additions) as shown in Fig. 9(b) and Table 2 $mSiO_2$/PTFE composites exhibit excellent low dielectric and low CTE performance, indicate that the $mSiO_2$/PTFE composites have excellent potential for practical applications.

4. Conclusions

In summary, this paper proposes a novel interface structure strategy of physical interaction to improve the interfacial combination between filler and matrix. Specifically, $mSiO_2$ is introduced as an inorganic filler, and the micro-mesoporous channels contained in $mSiO_2$ are utilized to achieve a tight interfacial combination with PTFE through the physical adsorption effect, to obtain $mSiO_2$/PTFE composites with excellent comprehensive performance. The microstructure, interfacial combination, dielectric, and thermal properties of the $mSiO_2$/PTFE composites were systematically studied. $mSiO_2$/PTFE has a tighter interfacial combination than $sSiO_2$/PTFE, as directly observed by FESEM and TEM. Furthermore, the thermomechanical (DSC and DMA) tests combined with the calculation of the crystallinity demonstrate that the $mSiO_2$/PTFE composites have good interfacial combinations. The physical interaction mechanism between $mSiO_2$ and PTFE is further revealed theoretically by mechanical analysis and solid mechanics modeling simulations. Compared with $sSiO_2$/PTFE, the CTE of $mSiO_2$/PTFE is reduced from 76 ppm $^{\circ}C^{-1}$ to 58 ppm $^{\circ}C^{-1}$ at 30 vol% of SiO_2 addition, while the ε_r and tan δ of $mSiO_2$/PTFE are decreased from 2.45 to 3.78×10^{-3} to 2.29 and 2.31×10^{-3} at 30 GHz. The fabricated $mSiO_2$/PTFE combines excellent low dielectric properties with low CTE, showing its great potential for applications in high-frequency and high-speed microwave communications.

Data availability statement

Data will be made available on request.

CRediT authorship contribution statement

Xin Li: Writing – original draft, Investigation, Conceptualization. **Jie Shen:** Validation. **Jing Zhou:** Validation. **Changqing Zhu:** Investigation. **Wen Chen:** Writing – review & editing, Supervision.

Declaration of competing interest

The authors declare that they have no known competing financial interests or personal relationships that could have appeared to influence the work reported in this paper.

Acknowledgements

This work was supported by Key Research and Development Project of Hubei Province (2021BAA214), and Natural Science Fund for Distinguished Young Scholars of Hubei Province (2021CFA067).

Appendix A. Supplementary data

Supplementary data to this article can be found online at https://doi.org/10.1016/j.heliyon.2024.e25442.

References

[1] Z. Zhou, K. Chen, X. Li, S. Zhang, Y. Wu, Y. Zhou, K. Meng, C. Sun, Q. He, W. Fan, E. Fan, Z. Lin, X. Tan, W. Deng, J. Yang, J. Chen, Sign-to-speech translation using machine-learning-assisted stretchable sensor arrays, Nat. Electron. 3 (2020) 571–578, https://doi.org/10.1038/s41928-020-0428-6.
[2] R. Song, X. Zhao, Z. Wang, H. Fu, K. Han, W. Qian, S. Wang, J. Shen, B. Mao, D. He, Sandwiched graphene clad laminate: a binder-free flexible printed circuit board for 5G antenna application, Adv. Eng. Mater. 22 (2020) 2000451–2000458, https://doi.org/10.1002/adem.202000451.
[3] A.C. Siegel, S.T. Phillips, M.D. Dickey, N. Lu, Z. Suo, G.M. Whitesides, Foldable printed circuit boards on paper substrates, Adv. Funct. Mater. 20 (2010) 28–35, https://doi.org/10.1002/adfm.200901363.
[4] S. Huang, P. Lin, H. Huang, L. Zhao, C. Zhu, Y. Yu, Z. Zhu, K. Nie, Q. Tang, L. Wang, H. Wang, Tailored polyphenylene sulfite composite with desirable mechanical performance and low dielectric constant by constructing a controllable aramid fiber network, Composites, Part B 201 (2020) 108334–108341, https://doi.org/10.1016/j.compositesb.2020.108334.
[5] H. Wang, H. Yang, Q.L. Wang, J.X. Tong, J.Y. Wen, Q.L. Zhang, Surface-modified $Li_3Mg_2NbO_6$ ceramic particles and hexagonal boron nitride sheets filled PTFE composites with high through-plane thermal conductivity and extremely low dielectric loss, Compos. Commun. 22 (2020) 100523–100529, https://doi.org/10.1016/j.coco.2020.100523.
[6] A. Huang, F. Liu, Z.X. Cui, H.K. Wang, X.C. Song, L.H. Geng, H.K. Wang, X.F. Peng, Novel PTFE/CNT composite nanofiber membranes with enhanced mechanical, crystalline, conductive, and dielectric properties fabricated by emulsion electrospinning and sintering, Compos. Sci. Technol. 214 (2021) 108980–108994, https://doi.org/10.1016/j.compscitech.2021.108980.
[7] C. Pan, K. Kou, Y. Zhang, Z. Li, G. Wu, Enhanced through-plane thermal conductivity of PTFE composites with hybrid fillers of hexagonal boron nitride platelets and aluminum nitride particles, Composites, Part B 153 (2018) 1–8, https://doi.org/10.1016/j.compositesb.2018.07.019.
[8] C. Riul, V. Tita, J. de Carvalho, R.B. Canto, Processing and mechanical properties evaluation of glass fiber-reinforced PTFE laminates, Compos. Sci. Technol. 72 (2012) 1451–1458, https://doi.org/10.1016/j.compscitech.2012.05.021.
[9] K.K. Han, J. Zhou, Q.Z. Li, J. Shen, Y.Y. Qi, X.P. Yao, W. Chen, Effect of filler structure on the dielectric and thermal properties of SiO_2/PTFE composites, J. Mater. Sci. Mater. Electron. 31 (2020) 9196–9202, https://doi.org/10.1007/s10854-020-03449-w.
[10] Y.C. Chen, H.C. Lin, Y.D. Lee, The effects of phenyltrimethoxysilane coupling agents on the properties of PTFE/silica composites, J. Polym. Res. 11 (2004) 1–7, https://doi.org/10.1023/B:JPOL.0000021757.94577.a3.

[11] W. Jin, A. Li, Y. Li, Y. Yu, J. Shen, J. Zhou, W. Chen, Enhancing high-frequency dielectric and mechanical properties of SiO_2/PTFE composites from the interface fluorination, Ceram. Int. 48 (2022) 28512–28518, https://doi.org/10.1016/j.ceramint.2022.06.165.

[12] N. Wang, H.G. Wang, J.F. Ren, G. Gao, S.S. Chen, G.R. Zhao, Y.W. Yang, J.Q. Wang, Novel additive of PTFE@SiO_2 core-shell nanoparticles with superior water lubricating properties, Mater. Des. 195 (2020) 109069–109078, https://doi.org/10.1016/j.matdes.2020.109069.

[13] M.M. Sarr, T. Kosaka, Effect of cellulose nanofibers on the fracture toughness mode II of glass fiber/epoxy composite laminates, Heliyon 9 (2023), https://doi.org/10.1016/j.heliyon.2023.e13203, 13203-13213.

[14] W.Z. Wang, N. Li, S.H. Jin, N. Wang, H. Chao, Y. Chen, Effect of anionic carboxymethyl cellulose acetate butyrate on recrystallization and surface modification of energetic ion salt TKX-50 crystal, Colloids Surf., A 645 (2022) 128885–128894, https://doi.org/10.1016/j.colsurfa.2022.128885.

[15] F.C. Luo, B. Tang, Z.X. Fang, Y. Yuan, H. Li, S.R. Zhang, Polytetrafluoroethylene based, F8261 modified realization of $Li_2SnMg_{0.5}O_{3.5}$ filled composites, Appl. Surf. Sci. 503 (2020) 144088–144094, https://doi.org/10.1016/j.apsusc.2019.144088.

[16] Y. Zhang, R.K. Wang, X.L. Zhang, S.Y. Guo, Ingenious sandwich-like adhesive films and controllable introduction of fluorine-containing groups toward strong adhesive strength and low dielectric characteristics, Ind. Eng. Chem. Res. 61 (2022) 14494–14507, https://doi.org/10.1021/acs.iecr.2c02150.

[17] H.D. Sun, L.X. Pang, Y.L. Ding, B.D. Xing, Y.J. Tang, X. Sun, J.C. Yuan, l. Zhou, Y.F. Wang, Y.C. Lyu, F. Sha, Influence of the physical morphological characteristics of mineral fillers on the bitumen-filler interfacial interaction, Construct. Build. Mater. 378 (2023) 131206–131218, https://doi.org/10.1016/j.conbuildmat.2023.131206.

[18] M.T. Run, S.Z. Wu, S.Y. Zhang, G. Wu, A polymer/mesoporous molecular sieve composite: preparation, structure and properties, Mater. Chem. Phys. 105 (2007) 341–347, https://doi.org/10.1016/j.matchemphys.2007.04.070.

[19] C.B. Yu, T. Wu, F.H. Yang, W.H. Rao, H.B. Zhao, Z.M. Zhu, Construction of hetero-structured nanohybrid relying on reactive phosphazene towards flame retardation and mechanical enhancement of epoxy resins, Eur. Polym. J. 167 (2022) 111075–111086, https://doi.org/10.1016/j.eurpolymj.2022.111075.

[20] X. Lei, B. Yu, H.L. Cong, C. Tian, Y.Z. Wang, Q.B. Wang, C.K. Liu, Synthesis of monodisperse silica microspheres by a modified stöber method, Integrated Ferroelectrics Int. J. 154 (2014) 142–146, https://doi.org/10.1080/10584587.2014.904651.

[21] K. Lan, Y. Xia, R.C. Wang, X.M. Zhang, A. Elzatahry, D.Y. Zhao, Confined interfacial monomicelle assembly for precisely controlled coating of single-layered titania mesopores, Matter 1 (2019) 527–538, https://doi.org/10.1016/j.matt.2019.03.003.

[22] E.Y. Trofimova, D.A. Kurdyukov, S.A. Yakovlev, D.A. Kirilenko, Y.A. Kukushkina, A.V. Nashchekin, A.A. Sitnikova, M.A. Yagovkina, V.G. Golubev, Monodisperse spherical mesoporous silica particles: fast synthesis procedure and fabrication of photonic-crystal films, Nanotechnology 24 (2013) 155601–155611, https://doi.org/10.1088/0957-4484/24/15/155601.

[23] A.M. Zhang, J.L. Chai, C.X. Yang, J.C. Zhao, G.Q. Zhao, G.L. Wang, Fibrosis mechanism, crystallization behavior and mechanical properties of in-situ fibrillary PTFE reinforced PP composites, Mater. Des. 211 (2021) 110157–110170, https://doi.org/10.1016/j.matdes.2021.110157.

[24] E.N. Brown, C.P. Trujillo, G.T. Gray, P.J. Rae, N.K. Bourne, Soft recovery of polytetrafluoroethylene shocked through the crystalline phase II-III transition, J. Appl. Phys. 101 (2007) 24916–24925, https://doi.org/10.1063/1.2424536.

[25] S.Q. Huang, P.L. Lin, H. Huang, L. Zhao, C.Q. Zhu, Y. Yu, Z.M. Zhu, K. Nie, Q.Q. Tang, L.X. Wang, H. Wang, Tailored polyphenylene sulfite composite with desirable mechanical performance and low dielectric constant by constructing a controllable aramid fiber network, Composites, Part B 201 (2020), https://doi.org/10.1016/j.compositesb.2020.108334, 108334–10841.

[26] Y. Yuan, D.D. Yu, Y.T. Yin, B. Tang, E.Z. Li, S.R. Zhang, Effect of sintering temperature on the crystallization behavior and properties of silica filled PTFE composites, J. Mater. Sci. Mater. Electron. 27 (2016) 13288–13293, https://doi.org/10.1007/s10854-016-5477-2.

[27] J.C. Wang, Z.H. Shen, J.Y. Jiang, J. Wang, X. Zhang, J. Shen, Y. Shen, W. Chen, L.Q. Chen, C.W. Nan, High-throughput finite-element design of dielectric composites for high-frequency copper clad laminates, Compos. Sci. Technol. 225 (2022) 109517–109524, https://doi.org/10.1016/j.compscitech.2022.109517.

[28] A. Zhang, J.L. Chai, C.X. Yang, J.H. Zhao, G.Q. Zhao, G.L. Wang, Fibrosis mechanism, crystallization behavior and mechanical properties of in-situ fibrillary PTFE reinforced PP composites, Mater. Des. 211 (2021) 110157–110170, https://doi.org/10.1016/j.matdes.2021.110157.

[29] K. Kato, Y. Ikeda, K. Ito, Direct determination of cross-link density and its correlation with the elastic modulus of a gel with slidable cross-links, ACS Macro Lett. 8 (2019) 700–704, https://doi.org/10.1021/acsmacrolett.9b00238.

[30] D.D. Luo, H.Y. Wu, H.X. Li, W.F. Zhang, L.Q. Zhang, Y.Y. Gao, Effect of shape and size of nanofillers on the viscoelasticity of polymer nanocomposites, Polymer 246 (2022) 124750–124760, https://doi.org/10.1016/j.polymer.2022.124750.

[31] C. Lang, M.P. Lettinga, Shear flow behavior of bidisperse rodlike colloids, Macromolecules 53 (2020) 2662–2668, https://doi.org/10.1021/acs.macromol.9b02239.

[32] Y.Y. Li, J. Zhou, J. Shen, Q.Z. Li, Y.Y. Qi, W. Chen, Ultra-low permittivity HSM/PTFE composites for high-frequency microwave circuit application, J. Mater. Sci. Mater. Electron. 33 (2022) 10096–10103, https://doi.org/10.1007/s10854-022-07999-z.

[33] Y.Y. Yu, D.J. Hou, J.J. Zhou, J. Shen, P.C. Zhang, W. Chen, J. Zhou, Improved dispersion and interfacial interaction of SiO_2@polydopamine fillers in polytetrafluoroethylene composites for reduced thermal expansion and suppressed dielectric deterioration, Ceram. Int. 49 (2023) 21492–21501, https://doi.org/10.1016/j.ceramint.2023.03.282.

[34] H. Tian, X. Li, J. Yan, X. Yu, H. Liu, J. Li, G. Guo, Natural protein-based biocomposites with superior paramagnetism and microwave absorbing properties by incorporating nanosized Fe_2O_3, Macromol. Mater. Eng. 307 (2022) 2100748–2100757, https://doi.org/10.1002/mame.202100748.

[35] T.W. Cheng, H. Keskkula, D.R. Paul, Property and morphology relationships for ternary blends of polycarbonate, brittle polymers and an impact modifier, Polymer 33 (1992) 1606–1619, https://doi.org/10.1016/0032-3861(92)91056-8.

[36] L.S. Liu, M.Y. Zhao, X.Y. Pei, S.K. Liu, S.G. Luo, M.J. Yan, R.Q. Shao, Y. Sun, W. Xu, Z.W. Xu, Improving corrosion resistance of epoxy coating by optimizing the stress distribution and dispersion of SiO_2 filler, Prog. Org. Coating 179 (2023) 107522–107532, https://doi.org/10.1016/j.porgcoat.2023.107522.

[37] D. Cao, W.Y. Zhou, M. Zhang, G.Z. Cao, Y.T. Yang, G.H. Wang, D.F. Liu, F.X. Chen, Insights into synchronously enhanced dielectric properties and thermal conductivity of β-SiC_w/PVDF nanocomposites by building a crystalline SiO_2 shell as an interlayer, Ind. Eng. Chem. Res. 61 (2022) 8043–8056, https://doi.org/10.1021/acs.iecr.2c01026.

[38] F.H. Liu, Y.H. Jin, J.Y. Li, W. Jiang, W.W. Zhao, Improved coefficient thermal expansion and mechanical properties of PTFE composites for high-frequency communication, Compos. Sci. Technol. 241 (2023) 110142–110148, https://doi.org/10.1016/j.compscitech.2023.110142.

[39] Y.H. Kim, Y.W. Lim, Y.H. Kim, B.S. Bae, Thermally stable siloxane hybrid matrix with low dielectric loss for copper-clad laminates for high-frequency applications, ACS Appl. Mater. Interfaces 8 (2016) 8335–8340, https://doi.org/10.1021/acsami.6b01497.

[40] T.J. Liu, M.C. Sil, C.M. Chen, Well-organized organosilane composites for adhesion enhancement of heterojunctions, Compos. Sci. Technol. 193 (2020) 108135–108145, https://doi.org/10.1016/j.compscitech.2020.108135.

[41] T.S. Sasikala, M.T. Sebastian, Mechanical, thermal and microwave dielectric properties of Mg_2SiO_4 filled polyteterafluoroethylene composites, Ceram. Int. 42 (2016) 7551–7563, https://doi.org/10.1016/j.ceramint.2016.01.162.

[42] Y.C. Chen, H.C. Lin, Y.D. Lee, The effects of filler content and size on the properties of PTFE/SiO_2 composites, J. Polym. Res. 10 (2003) 247–258, https://doi.org/10.1023/B:JPOL.0000004620.71900.16.

[43] H. Wang, F.M. Zhou, J.M. Guo, H. Yang, J.X. Tong, Q.L. Zhang, Modified BCZN particles filled PTFE composites with high dielectric constant and low loss for microwave substrate applications, Ceram. Int. 46 (2020) 7531–7540, https://doi.org/10.1016/j.ceramint.2019.11.252.

[44] S. Thomas, S. Raman, P. Mohanan, M.T. Sebastian, Effect of coupling agent on the thermal and dielectric properties of PTFE/$Sm_2Si_2O_7$ composites, Compos. Part A Appl. S. 41 (2010) 1148–1155, https://doi.org/10.1016/j.compositesa.2010.04.013.

[45] L. Zheng, J. Zhou, J. Shen, W. Chen, Y.Y. Qi, S.L. Shen, S. Li, The dielectric properties and dielectric mechanism of perovskite ceramic CLST/PTFE composites, J. Mater. Sci. Mater. Electron. 28 (2017) 11665–11670, https://doi.org/10.1007/s10854-017-6969-4.

[46] S. Thomas, V.N. Deepu, P. Mohanan, M.T. Sebastia, Effect of filler content on the dielectric properties of PTFE/$ZnAl_2O_4$-TiO_2 composites, J. Am. Ceram. Soc. 91 (2008) 1971–1975, https://doi.org/10.1111/j.1551-2916.2008.02365.x.

[47] F.C. Fu, B. Tang, Z.X. Fang, Y. Yuan, H. Li, S.R. Zhang, Effects of coupling agent on dielectric properties of PTFE based and $Li_2Mg_3TiO_6$ filled composites, Ceram. Int. 45 (2019) 20458–20464, https://doi.org/10.1016/j.ceramint.2019.07.023.

[48] S. Rajesh, V.S. Nisa, K.P. Murali, R. Ratheesh, Microwave dielectric properties of PTFE/rutile nanocomposites, J. Alloys Compd. 477 (2009) 677–682, https://doi.org/10.1016/j.jallcom.2008.10.092.